crystals

MDPI

Article

Electrosynthesis of Co-ZIF Using Bio-Derived Solvents: Electrochemical Evaluation of Synthesised MOFs as a Binder-Free Supercapacitor Electrode in Alkaline Electrolyte

Vijayakumar Manavalan [1,2], Brad Coward [2], Vesna Najdanovic-Visak [1] and Stephen D. Worrall [2,*]

[1] Energy & Bioproducts Research Institute, Aston University, Birmingham B4 7ET, UK; 210324576@aston.ac.uk (V.M.); v.najdanovic@aston.ac.uk (V.N.-V.)
[2] Aston Advanced Materials Research Centre, Aston University, Birmingham B4 7ET, UK; cowardb@aston.ac.uk
* Correspondence: s.worrall@aston.ac.uk

Abstract: Supercapacitors hold promise for energy storage due to their exceptional power density and fast charge/discharge cycles. However, their performance hinges on the electrode material. Zeolitic imidazolate frameworks (ZIFs) are attractive options due to their tailorable structure and high surface area. But traditional ZIF synthesis relies on toxic solvents derived from fossil fuels, hindering their envisioned environmental benefit. This study explores using bio-derived solvents for a greener and potentially superior approach. The researchers employed anodic electrodeposition to synthesise cobalt-based ZIFs (Co-ZIFs) as supercapacitor electrode materials. Two linkers (2-methylimidazole and benzimidazole) and two bio-derived solvents (Cyrene^{TM} and γ-valerolactone (GVL)) were investigated. X-ray diffraction analysis revealed that bio-derived solvents enhanced the crystallinity of Co-ZIFs compared to traditional solvents. Notably, Cyrene^{TM} promoted better crystallinity for Co-bIM/Co-mIM structures. The Full Width at Half Maximum (FWHM) analysis suggests Cyrene^{TM} promotes Co-bIM/Co-mIM crystallinity (lower FWHM). Co-mIM in Cyrene^{TM} exhibits the best crystallinity (FWHM = 0.233) compared to other ZIF samples. Scanning electron microscopy confirmed these findings, showing larger and well-defined crystals for bio-derived solvent-synthesised ZIFs. The choice of solvent significantly impacted the final ZIF structure. While 2-methylimidazole consistently formed ZIF-67 regardless of the solvent, benzimidazole exhibited solvent-dependent behaviour. GVL yielded the highly porous Co-ZIF-12 structure, whereas DMF (N,N-dimethylformamide) and Cyrene^{TM} produced the less porous ZIF-9. This work reports the first-ever instance of ZIF-12 synthesis via an electrochemical method, highlighting the crucial interplay between solvent and precursor molecule in determining the final ZIF product. The synthesised binder-free Co-ZIF electrodes were evaluated for supercapacitor performance. The capacitance data revealed GVL as the most effective solvent, followed by DMF and then Cyrene^{TM}. This suggests GVL is the preferred choice for this reaction due to its superior performance. The ZIF-12-based electrode exhibits an impressive specific capacitance (C_{sp}) of 44 F g^{-1}, significantly higher than those achieved by ZIF-9-Cyrene (1.2 F g^{-1}), ZIF-9-DMF (2.5 F g^{-1}), ZIF-67-GVL (35 F g^{-1}), ZIF-67-Cyrene (6 F g^{-1}), and ZIF-67-DMF (16 F g^{-1}) at 1 A g^{-1}. This surpasses the C_{sp} of all other ZIFs studied, including high-performing ZIF-67(GVL). ZIF-12(GVL) maintained superior C_{sp} even at higher current densities, demonstrating exceptional rate capability. Among the bio-derived solvents, GVL outperformed Cyrene^{TM}. Notably, the Co-bIM in the GVL sample exhibited a ZIF-12-like structure, offering potential advantages due to its larger pores and potentially higher surface area compared to traditional ZIF-67 and ZIF-9 structures. This work presents a significant advancement in Co-ZIF synthesis. By utilising bio-derived solvents, it offers a more sustainable and potentially superior alternative. This paves the way for the eco-friendly production of Co-ZIFs with improved properties for supercapacitors, gas separation, catalysis, and other applications.

Keywords: electrosynthesis; cobalt-ZIFs; bio-derived solvents; supercapacitors; binder-free supercapacitor electrode; alkaline electrolyte

Citation: Manavalan, V.; Coward, B.; Najdanovic-Visak, V.; Worrall, S.D. Electrosynthesis of Co-ZIF Using Bio-Derived Solvents: Electrochemical Evaluation of Synthesised MOFs as a Binder-Free Supercapacitor Electrode in Alkaline Electrolyte. *Crystals* **2024**, *14*, 700. https://doi.org/10.3390/cryst14080700

Academic Editor: Faxing Wang

Received: 25 June 2024
Revised: 23 July 2024
Accepted: 24 July 2024
Published: 1 August 2024

1. Introduction

Environmental concerns, like ozone depletion, global warming, and resource depletion, pose a significant threat on a global scale. The increasing number of climate emergency declarations worldwide underscores the urgency of addressing this crisis [1,2]. Along with the environmental crisis, chemical industries rely heavily on solvents for major synthesis processes, but many traditional solvents are derived from petroleum products, which are finite resources [3,4]. These petroleum-based solvents can pose health and environmental risks [3,5]. Thankfully, in recent years, more focus on environmental health and safety has grown among researchers and scientists [4]. Green chemistry, a sustainable approach to chemical processes, is gaining significant attraction [6–8]. As environmental awareness rises, the principles of green chemistry are finding wider applications across various fields [4,7,8]. Bio-based options like bioethanol, glycerol, dihydrolevoglucosenone (Cyrene^{TM}), and γ-valerolactone (γ-GVL) offer alternative replacements for fossil fuel-based solvents [9,10]. The toxicity of traditional fossil fuel-based solvents like N-methyl-2-pyrrolidone (NMP) and N,N-dimethylformamide (DMF) has led to their inclusion on the restricted substances list, significantly restricting their industrial use [4]. Although dimethyl sulfoxide (DMSO) offers a safer alternative to these, it still poses potential health risks [4–6]. Dihydrolevoglucosenone (Cyrene^{TM}) and γ-valerolactone (γ-GVL) emerge as the most promising bio-based substitutes for dipolar aprotic solvents [11,12]. Choosing a solvent for organic synthesis involves balancing cost with performance. While GVL (GBP 121/L) and Cyrene^{TM} (GBP 207/L) are pricier than DMF (GBP 60/L), their recyclability (high boiling points) and potentially lower consumption per reaction (less evaporation) could offer long-term economic benefits [4]. Additionally, their lower toxicity might simplify downstream processing. However, to quantify these advantages, research is needed to assess cost savings across various reactions compared to traditional solvents.

Supercapacitors, on the other hand, are rapidly gaining traction as attractive energy storage solutions due to their exceptional power density, enabling rapid charge and discharge cycles and extended lifespans [13,14]. However, their performance hinges on the selection of suitable electrode materials. Metal–organic frameworks (MOFs) have emerged as promising candidates for supercapacitor electrodes [15–18]. Metal–organic frameworks (MOFs), particularly a subgroup known as zeolitic imidazolate frameworks (ZIFs), are materials that rely on unsustainable solvents during synthesis, including N,N-dimethylformamide (DMF), dichloromethane (DCM), and benzene. These solvents are often toxic and volatile and contribute to environmental problems [19]. MOFs are constructed from metal ions, or clusters of metal ions, linked together by organic molecules containing heteroatoms [20,21]. These strong coordination bonds create intricate, three-dimensional structures with well-defined pores [22–24].

MOFs are revolutionising the world of supercapacitors due to their unique properties. Unlike traditional capacitors with limited storage, MOFs boast exceptional porosity and high surface area. This allows for efficient storage of electrolyte ions, the workhorses of supercapacitance. Moreover, MOFs offer unparalleled control over pore size and shape. These customisable pores can be precisely tailored to match the size of the electrolyte ions, maximising their accessibility and leading to faster charging and discharging cycles [25,26]. This exceptional material versatility is another key advantage. MOFs can be constructed like intricate molecular building sets. Scientists can choose from a vast library of organic linkers and metal centres to create MOFs with specific functionalities. This allows for the creation of MOFs specifically designed to enhance supercapacitor performance. For instance, certain metal centres can promote faster electron transfer within the MOF, leading to improved conductivity and overall performance. With these combined advantages, MOFs are poised to become the next-generation supercapacitor material, bridging the gap between conventional capacitors and batteries by offering superior energy storage with faster charging and discharging capabilities [27].

Metal–organic frameworks (MOFs) boast exceptional properties, making them ideal candidates for supercapacitors. However, MOFs must be incorporated as electrode coatings

to realise their full potential. In this configuration, their unique characteristics directly translate to enhanced supercapacitor performance. To achieve this, we employ electrochemical synthesis, a technique that delivers MOFs in a form perfectly suited for supercapacitor testing. Electrochemical synthesis stands out for its advantages in creating supercapacitor electrodes. Unlike traditional methods that require additional steps to form electrodes after MOF synthesis, this technique deposits MOFs directly onto a metal electrode in a single step. This not only simplifies the process but also ensures a robust connection between the MOF and the electrode.

Furthermore, electrochemical synthesis offers precise control over the morphology, or shape and size, of the MOF film. This allows for fine-tuning of crucial factors like pore accessibility and surface area, both of which significantly impact supercapacitor performance. By employing this technique, we aim to create MOFs in their ideal form for supercapacitor testing, paving the way for a new generation of energy storage devices [28–30].

Traditionally, MOF synthesis relies on solvents like N,N-dimethylformamide (DMF), which pose significant health and environmental risks [31,32]. Bio-derived solvents offer a compelling alternative as they are biodegradable and less harmful [33]. Additionally, these eco-friendly solvents can influence the morphology and crystallinity of MOFs, potentially leading to improved performance in electrochemical applications [27]. Also, the previous study suggests that the larger bio-solvent molecules might influence the final MOF structure during synthesis [27]. This study focuses on the anodic electrosynthesis of cobalt-based ZIFs (ZIF-67, ZIF-9, and ZIF-12) for supercapacitor electrodes, specifically exploring the use of bio-derived solvents (Cyrene^{TM} and GVL) as greener alternatives to DMF. Our primary goals are to minimise the environmental footprint by adopting bio-derived solvents and to investigate the potential enhancement of electrode performance through their influence on ZIF morphology and crystallinity.

Building upon the advantages of electrochemical synthesis for MOF electrode formation, this study further investigates the viability of replacing conventional, toxic solvents derived from fossil fuels with more sustainable alternatives. We evaluate the performance of the MOFs synthesised using these bio-based solvents as electrode materials for energy storage devices. This study explores bio-derived solvents (Cyrene^{TM} and γ-valerolactone) as a sustainable alternative to traditional solvents in the electrochemical synthesis of Co-ZIF materials for supercapacitor applications. We investigate the performance of these bio-derived MOFs as electrode materials and compare them to those synthesised using conventional methods. This research addresses the environmental concerns associated with traditional solvent use while exploring the potential of bio-derived alternatives for high-performance supercapacitors.

2. Materials and Methods

2.1. Materials for Synthesis

To synthesise Co-ZIFs in an electrochemical cell setup, the Co metal foil (99.9%) was bought from Advent Research Materials Ltd., Eynsham, Oxford, England and the materials 2-methyl imidazole (mIM) (99%), ethanol (HPLC grade), Cyrene^{TM}, (HPLC grade), GVL (HPLC grade), water (HPLC grade), N,N-dimethylformamide (DMF) (HPLC grade) were bought from Fisher Scientific, Loughborough, Leicestershire, United Kingdom and used throughout the process without any further purification. Furthermore, the supporting electrolyte tributylmethylammonium methyl sulphate (TBMAMS) (>95%) was purchased from Santa Cruz Biotechnology, Dallas, Texas, United States. For electrochemical testing, potassium hydroxide and Whatman Grade 1 Qualitative Filter Paper were purchased from Fisher Scientific, Loughborough, Leicestershire, United Kingdom and coin cell (CR2032) and hydraulic crimper were purchased from MTI Corporation, Richmond, California, USA.

2.2. Electrochemical Synthesis of Co-ZIF MOF Coating

Various Co-ZIF MOF coatings were synthesised electrochemically via the anodic deposition method. The setup consists of two metal foils (Co) submerged into an electrolyte

solution containing TBMAMS (0.06 mol dm^{-3}) as an electrolyte and 2-methylimidazole as a linker (3 mol dm^{-3}) to synthesise Co-mIM ZIFs. For Co-bIM ZIFs, the linker was replaced by benzimidazole (0.12 mol dm^{-3}) in the homogenous solution. The electrodes were ~10 cm^2 in area, held ~4 cm apart, and kept in a homogenous solution. An Autolab potentiostat (PGSTAT204, AUT50093) from Metrohm, Runcorn, Cheshire, United Kingdom was used to apply a fixed potential of 2.5 V between the two metal electrodes for a specified time and at a relevant temperature (°C) (Table 1), generating a Co-ZIF coating on the surface of the anode. After completion of the reaction time, the final coated electrodes were thoroughly rinsed and washed with ethanol to remove excess and unreacted linkers and electrolytes present on the surface of the electrode. Then, the electrodes were left for room drying for 24 h. Table 1 summarises the conditions used to form the Co-ZIF coatings utilising the DMF and bio-derived solvents Cyrene™ and GVL, respectively. Various optimisation conditions, such as linker concentration, organic solvent-to-water ratio, reaction temperature, and reaction time were evaluated. This rigorous optimisation process was conducted to obtain a quality coating of the MOF on the Co electrode.

Table 1. Summary of conditions for synthesis of Co-ZIF coating with DMF, Cyrene™, and GVL using bIM and mIM as a linker. The common parameters included metal electrode = cobalt, MTBAMS = 0.06 mol dm^{-3}, organic solvent/H_2O = 75/25 (Vol%), time = 180 min.

Linker Concentration (mol dm^{-3})	Solvent	Temperature (°C)
bIM 0.12	DMF	85
bIM 0.12	Cyrene™	100
bIM 0.12	GVL	85
mIM 3.0	DMF	85
mIM 3.0	Cyrene™	100
mIM 3.0	GVL	85

2.3. Characterisation of MOF Coatings

The crystallographic information of the MOF coatings was obtained via X-ray diffraction (XRD) using a Rigaku Miniflex X-ray diffractometer (Rigaku Europe SE, Neu-Isenburg, Germany). The XRD patterns were acquired from the coatings formed on top of the anode surface using Cu radiation at 40 kV and 15 mA in the range 3–35 $2\theta^0$. Data were backgrounded using the inbuilt background removal tool within the Smart Lab Studio software (version: 4.4.241.0) to remove the influence of the underlying metal electrode on the diffraction patterns. Scanning electron microscopy (SEM) analyses were conducted using a Quattro SEM (Thermo Fisher Scientific, Waltham, Massachusetts, USA). The operating parameters used for the study were high vacuum mode with an acceleration voltage of 10 kV and a spot size of 3, and the images were captured with a secondary electron detector.2.4. Preparation of the Electrodes and Electrochemical Measurements

A two-electrode configuration was used for all electrochemical measurements. The coated ZIFs (ZIF-67, ZIF-9, and ZIF-12) from the above synthesis were used as binder-free supercapacitor electrodes. Electrochemical measurements were conducted in sealed CR2032 coin cells with a symmetrical configuration. The electrodes were separated by Whatman Grade 1 Qualitative Filter Paper in an aqueous 6 M KOH electrolyte solution, which was employed for all cells. All the electrochemical tests were carried out in an Auto lab potentiostat (PGSTAT204, AUT50093). Cyclic voltammetry was carried out between 0 and 1.0 V potential range at various scan rates between 1 mV s^{-1} and 1000 mV s^{-1}.

Galvanostatic charge–discharge (GCD) was carried out between various applied currents between the voltage range from 0–1 V.

The gravimetric capacitance, C_{sp} (F g^{-1}), can be inferred from the CV plots using Equation (1):

$$C_{sp}(CV) = \frac{1}{2 \cdot s \cdot \Delta V \cdot m} \int Idv \quad (1)$$

where I is the current (A), V is the voltage (V), s is the sweep rate of the cyclic voltammogram (V s^{-1}), ΔV is the voltage range the sweep is carried within (V), and m is the mass of the electrode materials (g).

Using the GCD technique, the specific capacitance of each electrode was calculated by using Equation (2):

$$C_{sp}(GCD) = 4 \cdot \frac{I \cdot \Delta t}{m \cdot \Delta V} \quad (2)$$

where C_{sp}, I (A), Δt (s), m (g), and ΔV are the specific capacitance, discharge current, discharge time, the mass of the active material, and the total potential window, respectively.

3. Results

3.1. Synthesis of Co-mIM ZIFs Using Various Solvents

Different Co-mIM ZIFs were synthesised following the synthesis condition reported in Table 1 using an anodic electrodeposition method. A uniform thin film coating was obtained on each cobalt electrode using three different solvents. The coated electrodes were further characterised by using X-ray diffraction (XRD) and scanning electron microscope (SEM). Crystallographic analysis of the prepared samples was performed using XRD to assess their crystallinity and phase purity. Figure 1A–C represent the XRD patterns of the Co-mIM ZIFs synthesised in three different solvents in the presence of an mIM linker. The XRD pattern of the synthesised three MOFs coating exhibits the same crystalline phase ZIF-67, which is further confirmed by comparing the peak positions in the XRD patterns with predicted values from reference materials [34,35]. The XRD patterns exhibit diffraction peaks at 2θ values of 19.05°, 32.42°, 37.9°, and 38.9°, corresponding to (0 0 1), (1 0 0), (1 0 1) and (1 0 2) planes of hexagonal phase [35].

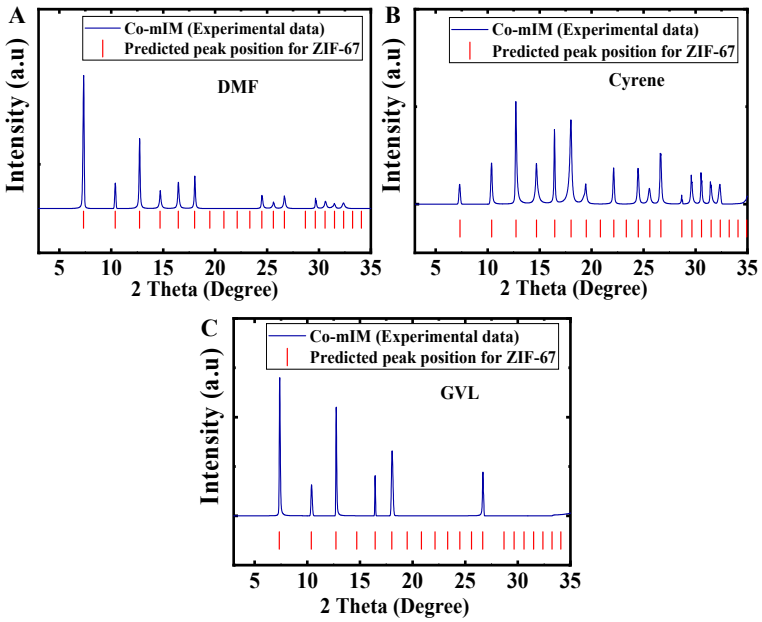

Figure 1. XRD patterns of Co-mIM ZIF coatings obtained using (**A**) DMF, (**B**) Cyrene™, and (**C**) GVL.

The scanning electron microscope (SEM) images in Figure 2A–C largely support the observations made from the XRD analysis for the Co-mIM ZIFs (Figure 1A–C). Figure 2A–C show that

the SEM images reveal Co-ZIF coatings obtained using different solvents (traditional and bio-derived) on the underlying electrode. While the SEM images suggest a more uniform and ordered arrangement of particles in MOF coatings prepared with GVL compared to DMF, they do not definitively show the same trend for Cyrene™. This observation aligns with the XRD data (Figure 1), where only GVL exhibited a lower FWHM value (potentially indicating better crystallinity) than DMF. The unique properties of bio-derived solvents like GVL may influence the MOF crystallisation process, promoting a more ordered arrangement of particles.

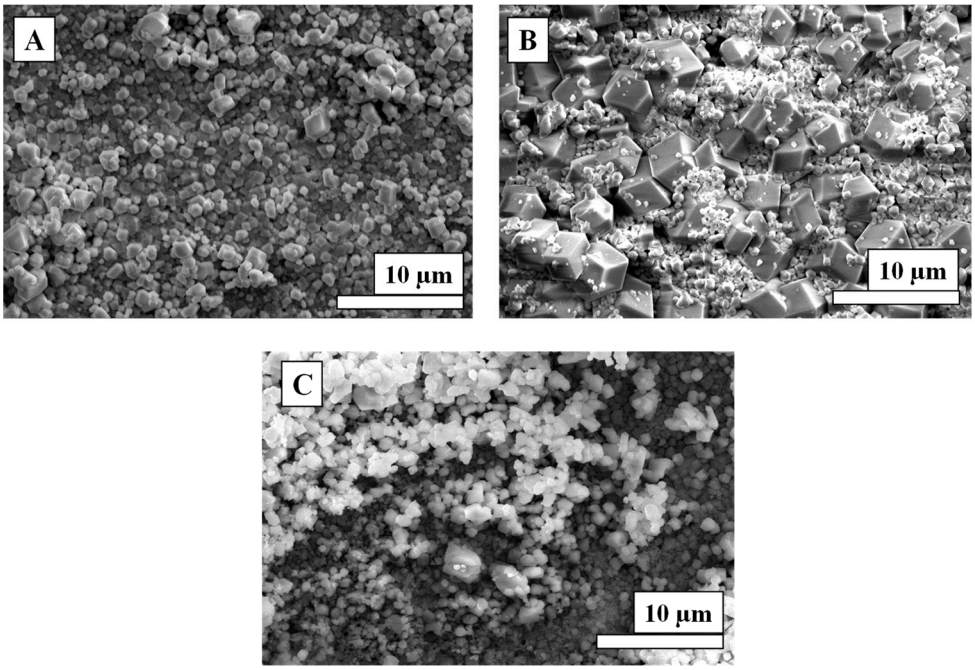

Figure 2. SEM image of Co-mIM ZIF coatings obtained using (**A**) DMF, (**B**) Cyrene™, and (**C**) GVL.

3.2. Synthesis of Co-bIM Using Various Solvents

Like the Co-mIm ZIF synthesis, Co-bIm ZIFs were synthesised by replacing the linker mIm with bIm in the reaction. The exact synthesis condition is mentioned in Table 1. Co-bIm ZIFs were synthesised in three different solvents (traditional (DMF) and bio-derived solvents (Cyrene™ and GVL)) to obtain the final coating on the cobalt electrode. Each solvent offers distinct advantages and disadvantages. Amongst various properties, viscosity plays an important role. Cyrene™ (45 mPa·s (at 25 °C)) has a higher viscosity than GVL (2.2 mPa·s (at 20 °C)) and DMF (0.79 mPa·s (at 20 °C)). Also, viscosity influences the ion transport processes during the reaction. For efficient ion transport movement, the temperature of Cyrene™ is raised to promote diffusion and ion transport processes during the reaction, potentially mitigating the limitations imposed by its higher viscosity compared to GVL and DMF. The final coated thin film ZIF electrodes were characterised using XRD and SEM for further analysis. From the synthesis, a uniform coating was observed for each of the electrodes from the reaction. Figure 3A shows that the XRD patterns are ZIF-9 for DMF, and Figure 3B shows the mixed pattern of ZIF-9 and ZIF-12 for Cyrene™, respectively.

Interestingly, for the GVL-based Co-bIM ZIF coating, an entirely different crystalline phase compared to traditional solvent and Cyrene™ is observed. This is evident from the previous report; in the case of Zn and bIM, rather than forming the SOD (sodalite) phase ZIF-7, the RHO phase ZIF-11 was obtained with high purity [36]. In the case of Co and bIM in GVL, rather than forming the SOD phase ZIF-9, the RHO phase ZIF-9 was obtained with high purity, which was previously reported by Doung et al. as ZIF 12 [37]. FWHM analysis of the XRD data suggests Cyrene™ as the most effective solvent for promoting

crystallinity in the ZIF-67, ZIF-9, and ZIF-12 frameworks. Lower FWHM values were consistently observed for samples synthesised in Cyrene™ compared to DMF and GVL.

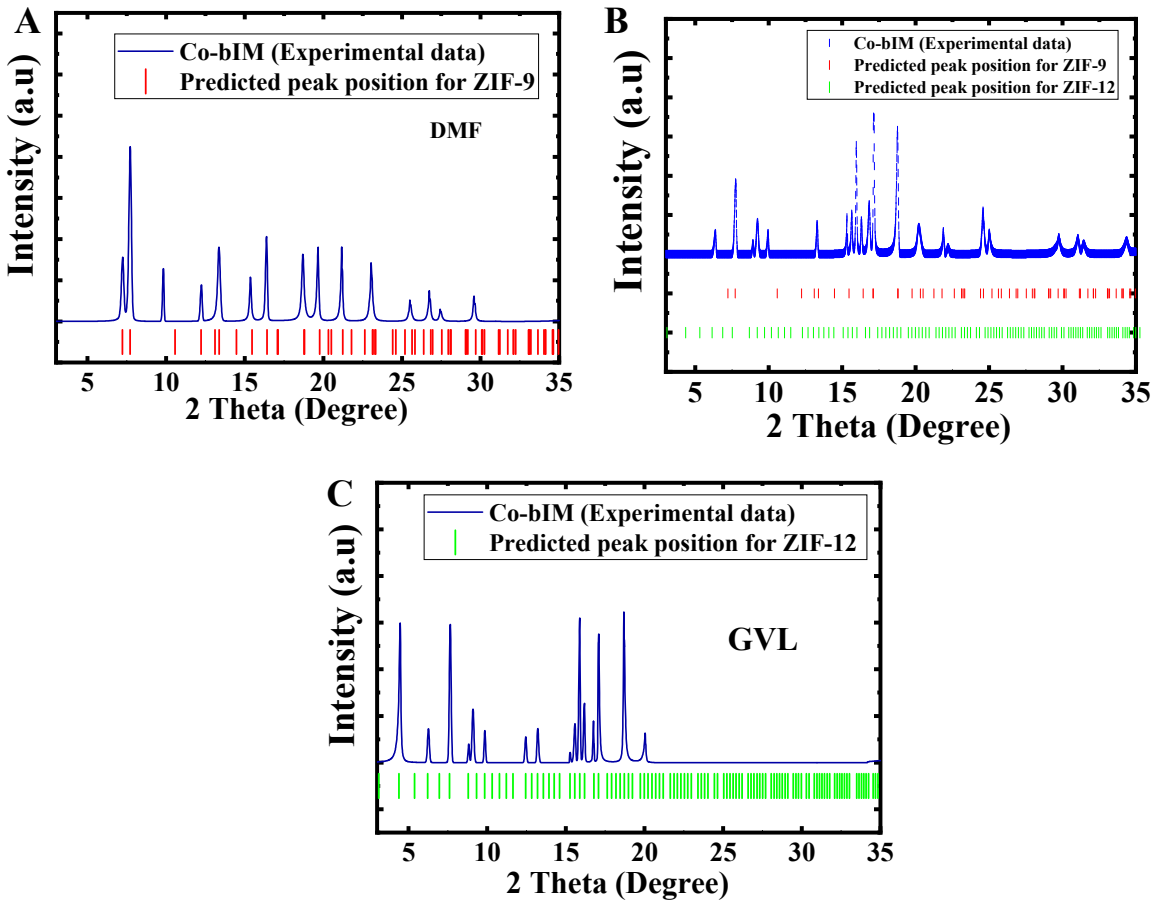

Figure 3. XRD patterns of Co-bIM ZIF coatings obtained using (**A**) DMF, (**B**) Cyrene™, and (**C**) GVL.

Conversely, DMF resulted in the broadest peaks for all frameworks, indicating potentially lower crystallinity. GVL showed mixed effects, promoting better crystallinity for ZIF-12 but performing less favourably for ZIF-67 and ZIF-9 than Cyrene. Among all samples, ZIF-67 synthesised in Cyrene™ exhibited the sharpest peak (FWHM = 0.233), suggesting it possesses the highest crystallinity and potentially the most well-defined crystal structure.

The SEM images of these coatings (Figure 4A–C) correlate with much of what was observed in the XRD data (Figure 3A–C). The observed crystal morphologies in Figure 4C are entirely different from those observed when using the same reactants with DMF and Cyrene™ as the solvent. Using GVL significantly improved the overall crystal quality of the MOF products. SEM analysis revealed the formation of well-faceted octahedral crystals with sharper edges for MOFs synthesised with GVL. This contrasts with the less defined morphologies observed in MOFs prepared using a conventional solvent. The use of GVL improved the overall crystal quality in two different MOF products, exhibiting clearly defined crystals with discernible morphologies in this case. From the SEM images, the average particle sizes were determined as follows: Co-mIM in DMF (2.18 µm), Cyrene™ (3.97 µm), and GVL (1.3 µm), and Co-bIM in DMF (2.03 µm), Cyrene™ (7.94 µm), and GVL (2.60 µm). Generally, GVL yielded the smallest particles for both Co-mIM and Co-bIM, followed by DMF and then Cyrene™. This suggests that GVL promotes the formation of smaller crystallites during synthesis.

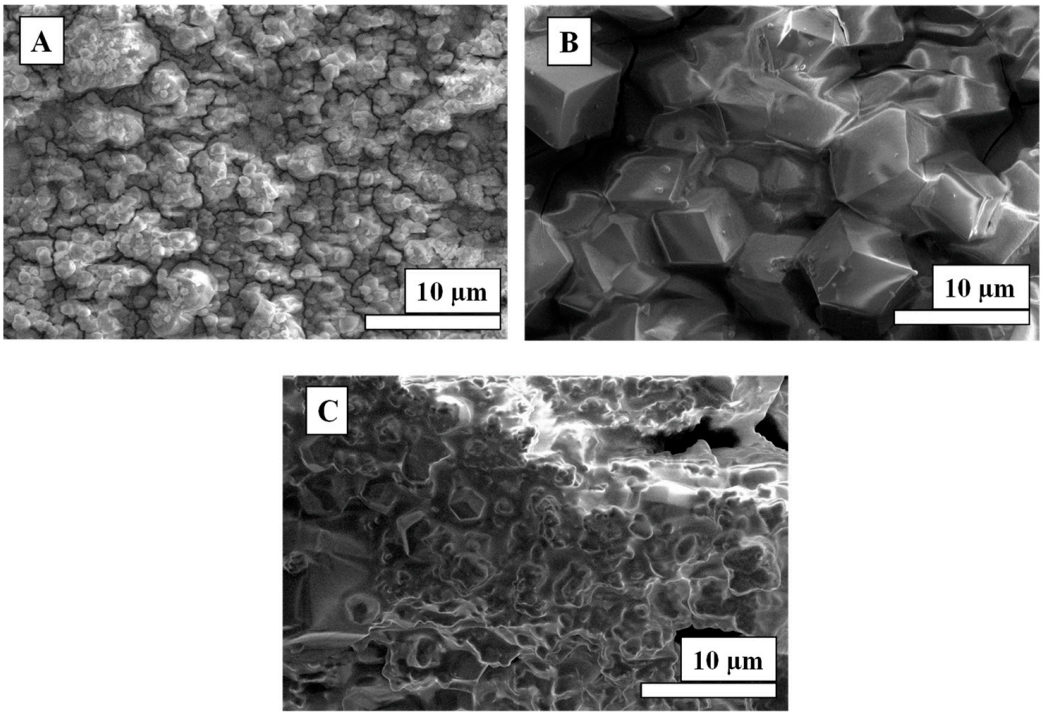

Figure 4. SEM image of Co-bIM ZIF coatings obtained using (**A**) DMF, (**B**) Cyrene^{TM}, and (**C**) GVL.

3.3. Cyclic Voltammetry

The synthesised electrodes were tested as an electrode material for supercapacitors using a two-electrode system in an alkaline electrolyte (6M KOH). Cyclic voltammetry (CV) is a powerful technique to understand the charge storage mechanisms of synthesised Co-ZIF electrode materials for supercapacitors. This study used the CV technique to investigate the electrochemical behaviour of ZIF-67, ZIF-9, and ZIF-12 electrodes. The two electrodes were scanned across a voltage range from 0 to 1.0 V at varying scan rates from 1.0 to 100 mV s^{-1} to access the active sites in the ZIFs. The cyclic voltammetry (CV) curves presented in Figure 5A–F provide insights into the charge storage mechanisms of the synthesised ZIF materials. Figure 5A–C depicts the CV profiles of ZIF-67 electrodes prepared using DMF, Cyrene^{TM}, and GVL as solvents. Similarly, Figure 5D,E shows the CV profiles for ZIF-9 electrodes synthesised with DMF and Cyrene^{TM}. Finally, Figure 5F presents the CV profile of the ZIF-12 electrode prepared using GVL.

Notably, redox peaks in the CV curves for all six ZIF systems at lower scan rates (1 mV s^{-1} to 5 mV s^{-1}) are a vital observation (Appendix A: Figure A1). The observed redox peaks in the CV curves likely correspond to the conversion of Co(II) to Co(III) within the ZIF framework, a well-established faradaic process reported in the previous literature for cobalt-based ZIFs [38]. These peaks indicate faradaic processes, where electron transfers occur between the ZIF framework and electrolyte ions. The redox peaks likely correspond to the intercalation/deintercalation of OH^- ions from the 6 M KOH electrolyte solution into the ZIF structure [39,40]. Lower scan rates allow for sufficient time for electrolyte ions to penetrate the porous structure of the ZIF electrodes and interact with the accessible active sites. This interaction facilitates ions' reversible adsorption/desorption, contributing to the overall capacitance. However, redox peaks fade significantly across all ZIF systems at higher scan rates (50 mV s^{-1} to 100 mV s^{-1}). This fading suggests a limitation in the ion diffusion kinetics at faster scan rates. The electrolyte ions likely lack sufficient time to fully access and interact with the active sites within the ZIF electrode framework. This phenomenon highlights the interplay between scan rate and ion diffusion kinetics, significantly impacting the overall charge storage performance.

Interestingly, the ZIF electrodes derived from bio-derived solvents (Cyrene^{TM} and GVL) exhibit a distinct advantage (Figure 5B,C,E,F). These electrodes demonstrate a more

pronounced retention of redox behaviour even at higher scan rates than those synthesised using DMF (Figure 5A,D). This observation can be attributed to the influence of bio-derived solvents on the structural properties and purity of the obtained MOF crystals. These solvents might promote the formation of highly crystalline and defect-free ZIF structures (ZIF-67 and ZIF-9) with well-defined pores. Such optimised structures offer improved pathways for electrolyte ion diffusion, even at faster scan rates, leading to better utilisation of active sites and enhanced rate capability.

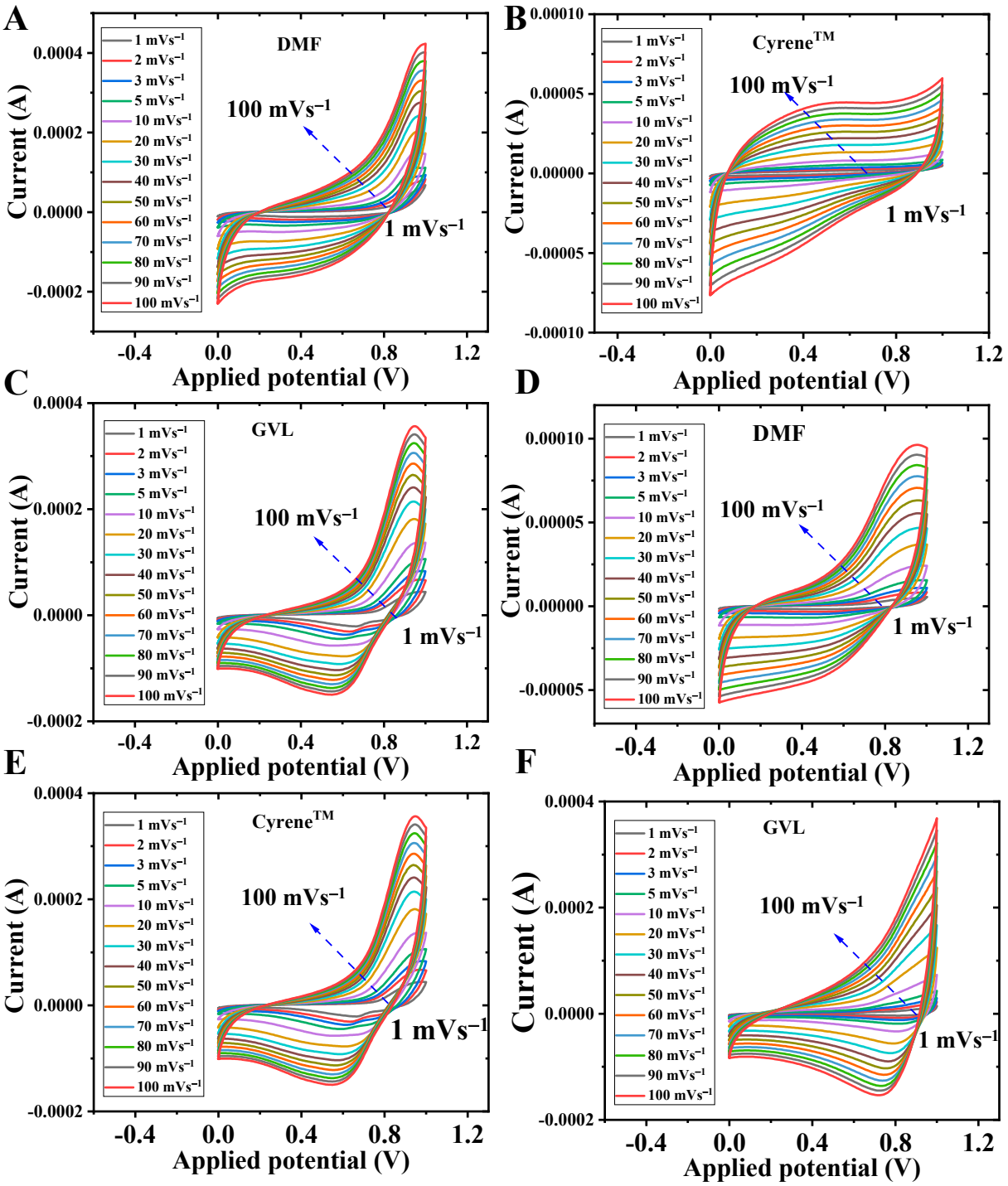

Figure 5. Cyclic voltammetry current vs. applied potential profile for Co-mIM ZIFs in (**A**) DMF, (**B**) Cyrene™, (**C**) GVL, and Co-bIM ZIFs in (**D**) DMF, (**E**) Cyrene™, and (**F**) GVL.

Furthermore, the ZIF-12 electrode, which possesses a different topological structure (RHO-type), stands out among the studied materials. While all ZIFs display redox behaviour, ZIF-12 exhibits a particularly enhanced electrochemical response (Figure 5F). This observation suggests that the intrinsic framework topology of ZIF-12 might play a crucial role in facilitating ion transport and promoting faradaic reactions. The RHO-type structure of ZIF-12 might offer inherent advantages in pore connectivity and accessibility, leading to superior electrochemical performance compared to the other synthesised ZIFs. Bio-derived solvents provide a promising approach for tailoring the structural properties of ZIFs, leading to improved rate capability by promoting electrolyte ion diffusion kinetics. Additionally, the framework topology plays a significant role, with ZIF-12 exhibiting enhanced electrochemical performance due to its intrinsic structural characteristics. These findings pave the way for designing and developing ZIF-based electrode materials with optimised charge storage properties for high-performance energy storage applications.

Figure 6A–F presents the capacitance profiles of the synthesised Co-ZIF electrodes evaluated in an alkaline electrolyte. This analysis complements the insights gained from the cyclic voltammetry (CV) measurements (Figure 5) and sheds light on the charge storage capabilities of the materials. Here, the capacitance is plotted against the operating voltage using equation.

Similar to the structural organisation in Figure 5, Figure 6A–C depict the capacitance profiles for ZIF-67 electrodes prepared with DMF, Cyrene^{TM}, and GVL, respectively. Likewise, Figure 6D–E show the profiles for ZIF-9 electrodes synthesised with DMF and Cyrene^{TM}. Finally, Figure 6F presents the capacitance profile of the ZIF-12 electrode prepared using GVL. A key observation from Figure 6 is the generally enhanced capacitance exhibited by ZIF electrodes, and the experimental data suggest an ordering of solvent effectiveness, with GVL (γ-valerolactone) exhibiting the greatest efficiency, followed by DMF (N,N-dimethylformamide) and Cyrene^{TM} being the least effective. This trend indicates that GVL may be the preferred choice for the investigated reaction due to its superior performance.

This trend aligns with the observations from the CV analysis (Figure 5), where bio-derived solvent-based ZIFs displayed better retention of redox peaks at higher scan rates, suggesting improved ion diffusion kinetics. Figure 6F further highlights the exceptional performance of the ZIF-12 electrode, which exhibits a larger capacitance area at higher operating potentials than other ZIFs. This observation can be attributed to the unique RHO-type topology of ZIF-12. This framework structure might offer inherent advantages regarding pore connectivity and accessibility. The arrangement of pores within the ZIF-12 framework might provide more favourable pathways for electrolyte ion diffusion, even at higher scan rates (as observed in the CV analysis).

Additionally, the specific geometry of the RHO-type structure could promote faradaic reactions to a greater extent, further contributing to the enhanced capacitance observed for ZIF-12. The findings from the capacitance analysis (Figure 6) are consistent with the observations from the CV measurements (Figure 5). Both data sets emphasise the crucial role of solvent choice and framework topology in influencing the charge storage behaviour of Co-ZIF electrodes. Bio-derived solvents present a promising strategy for tailoring ZIF structures to achieve improved capacitance by promoting well-defined pore structures and potentially facilitating faradaic reactions. Furthermore, the intrinsic framework topology plays a significant role, with ZIF-12 demonstrating superior performance due to its RHO-type structure, which likely enhances ion transport and faradaic processes.

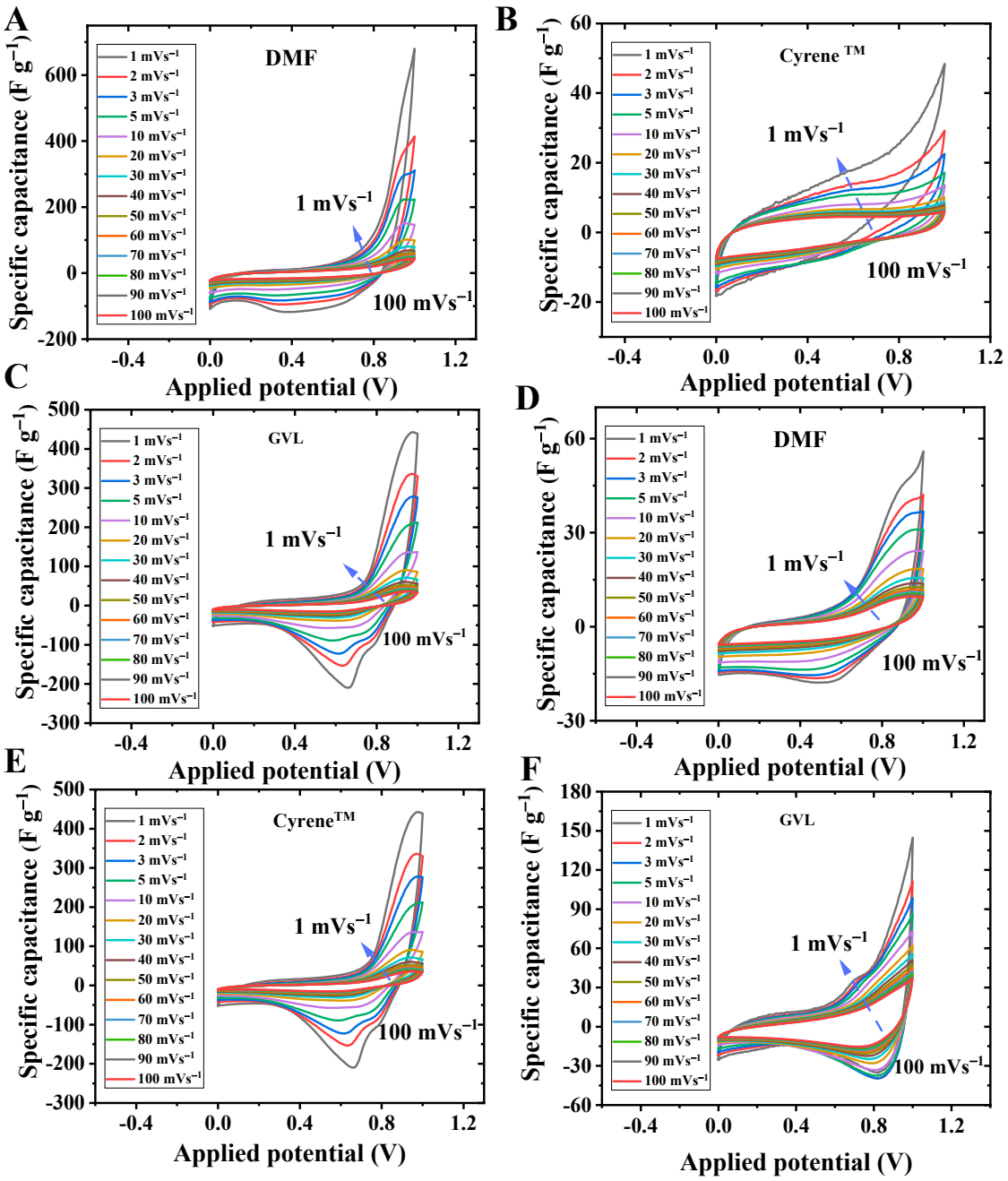

Figure 6. Specific capacitance vs. applied potential profile for Co-mIM ZIFs in (**A**) DMF, (**B**) Cyrene™, (**C**) GVL, and Co-bIM ZIFs in (**D**) DMF, (**E**) Cyrene™, and (**F**) GVL.

3.4. Galvanostatic Charge-Discharge

Understanding the interplay between material properties and electrochemical performance is crucial for optimising supercapacitor electrodes. Galvanostatic charge–discharge (GCD) measurements provide valuable insights into these materials' practical energy storage capabilities by directly evaluating their specific capacitance (C_{sp}) under various current densities. From the galvanostatic discharge curve, the specific capacitance is calculated by using Equation (2).

This study presents a comparative analysis of the GCD performance for a series of Co-ZIF (ZIF-67, ZIF-9, and ZIF-12) electrodes synthesised using different solvents (N,N-dimethylformamide (DMF), Cyrene™, and γ-valerolactone (GVL)). The results reveal a remarkable enhancement in C_{sp} for ZIF-12(GVL) compared to other ZIFs, highlighting the combined effect of solvent and framework on charge storage performance.

Impact of Solvent on ZIF-67 Electrodes:

The GCD data for ZIF-67 electrodes showcase a significant influence of the solvent employed during synthesis (Figure 7A–C). ZIF-67 synthesised with GVL (denoted as ZIF-67(GVL) in Figure 7C) exhibits the highest C_{sp} values across all tested currents (1 A g^{-1} to 15 A g^{-1}) compared to those prepared with DMF and Cyrene^{TM} (denoted as ZIF-67(DMF) and ZIF-67(Cyrene), respectively). Notably, ZIF-67(GVL) demonstrates a maximum C_{sp} of 39 F g^{-1} at 1 A g^{-1}, which is nearly 2.4 times greater than ZIF-67(DMF) (16 F g^{-1}) and over six times higher than ZIF-67(Cyrene) (6 F g^{-1}). This trend persists at higher current densities, with ZIF-67(GVL) maintaining a C_{sp} of 10 F g^{-1} at 15 A g^{-1}, exceeding ZIF-67(DMF) (5.5 F g^{-1}) and ZIF-67(Cyrene) (2.5 F g^{-1}), respectively.

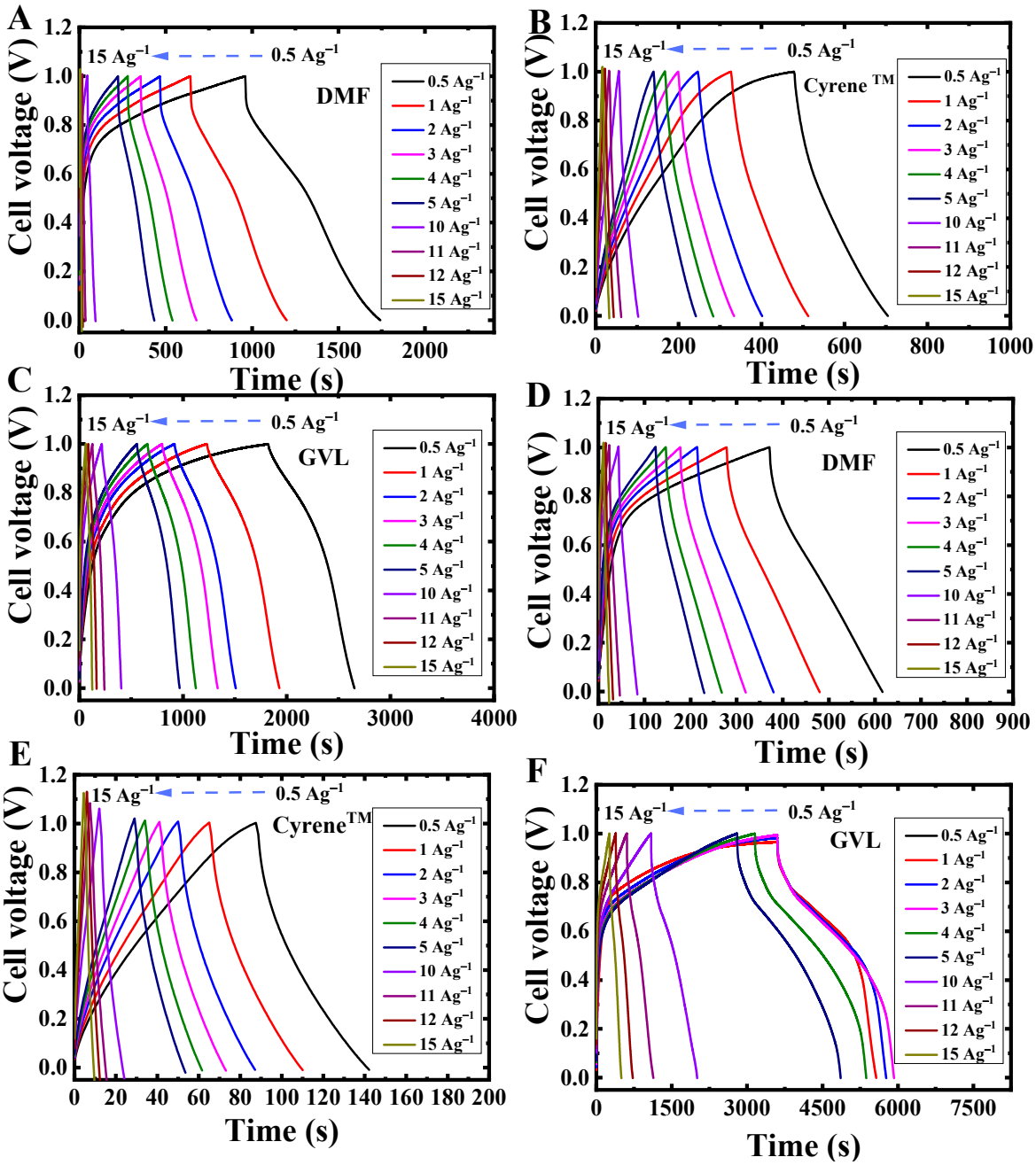

Figure 7. Galvanostatic charge–discharge profile for Co-mIM ZIFs in (**A**) DMF, (**B**) Cyrene^{TM}, (**C**) GVL, and Co-bIM ZIFs in (**D**) DMF, (**E**) Cyrene^{TM}, and (**F**) GVL.

The observed enhancement in C_{sp} for ZIF-67(GVL) can be attributed to the potential influence of the bio-derived solvent GVL on the ZIF-67 framework formation. Bio-solvent (GVL) might promote the development of highly crystalline structures with well-defined and interconnected pores. These optimised structures offer a larger effective surface area for efficient electrolyte ion adsorption and charge storage. This aligns with the previous report [12,27] suggesting that bio-derived solvents can influence the crystallisation process of metal–organic frameworks (MOFs), improving porosity and enhancing electrochemical performance.

Performance of ZIF-9 Electrodes:

The GCD analysis for ZIF-9 electrodes reveals a generally lower C_{sp} to ZIF-67 (Figure 7D,E). ZIF-9(DMF) exhibits the highest C_{sp} among ZIF-9 electrodes, reaching a maximum of 2.5 F g^{-1} at 1 A g^{-1}. Like ZIF-67, ZIF-9 electrodes synthesised with Cyrene^{TM} display lower C_{sp} values than DMF and GVL counterparts. This observation suggests that the intrinsic framework structure of ZIF-9 might inherently offer a lower capacitance to ZIF-67. The ZIF materials exhibited a clear correlation between surface area and capacitance. ZIF-67, with a significantly higher surface area (1700 m^2 g^{-1}) [41] compared to ZIF-9 (413.0 m^2 g^{-1}) [42], displayed superior capacitive performance. This observation aligns with supercapacitor storage performance, where a larger surface area provides more accessible sites for electrolyte ion adsorption, leading to increased charge storage capability [43,44]. The enhanced capacitance in ZIF-67 can be attributed to its highly porous structure, allowing for efficient electrolyte penetration and maximising its accessible surface area.

ZIF-12: The Outperformer with RHO-Type Topology:

The ZIF-12 electrode prepared with GVL (denoted as ZIF-12(GVL)) stands out amongst all studied ZIFs, demonstrating exceptional C_{sp} values throughout the tested current range (Figure 7F). ZIF-12(GVL) delivers a maximum C_{sp} of 44 F g^{-1} at 1 A g^{-1}, which is superior to the best-performing ZIF-67(GVL) and significantly surpasses the C_{sp} of all other ZIF-9 and ZIF-67 variants under similar conditions. Even at higher current densities, ZIF-12(GVL) retains a superior C_{sp}, with a 15 F g^{-1} value at 15 A g^{-1}. This represents a performance enhancement compared to ZIF-67(GVL) (10 F g^{-1}) and ZIF-67(DMF) (2.5 F g^{-1}), respectively. ZIF-12 possesses a high specific surface area (1810 m^2 g^{-1} [45]), exceeding those of ZIF-67 and ZIF-9. This characteristic likely contributes to its enhanced supercapacitor performance by providing more accessible sites for electrolyte ion adsorption and promoting efficient charge storage.

From the CV and GCD profile, the initial cycles, especially at lower currents, can cause slight asymmetries in electrochemical profiles due to minor, somewhat irreversible, material changes and internal cell resistances. High average coulombic efficiency (>50% at low current, >95% at high) indicates good overall reversibility despite these initial effects (Figure A2). It reflects balanced charge exchange over many cycles, with minimal losses despite potential initial asymmetries. Also, the rate performance of the sample ZIF-12 is evaluated by conducting a cycling test (number of cycles vs. capacitance retention) of the supercapacitor cell. It was observed that the ZIF-12-based supercapacitor exhibits a very good cycling performance upon 1000 charge–discharge cycles with 99% of capacitance retention and also 99% coulombic efficiency (Figure A3).

4. Discussion

This study investigates the influence of solvent choice on the supercapacitor performance of various cobalt ZIFs synthesised using different linkers and solvents. Six cobalt ZIF samples were synthesised using cobalt metal electrodes and two linkers: methylimidazole (mIM) and benzimidazole (bIM). Three different solvents were employed for the synthesis: N,N-dimethylformamide (DMF), Cyrene^{TM} (dihydrolevoglucosenone), and γ-valerolactone (GVL). These samples were then evaluated as electrode materials for supercapacitors in a 6 M KOH electrolyte. The choice of linker and solvent plays a crucial role in determining the ZIF structure and its properties. In this study, the samples synthesised

with mIM as the linker are likely to exhibit the ZIF-67 structure, and those with bIM as the linker are likely to exhibit the ZIF-9 structure. However, the cobalt ZIF with bIM in GVL has a different structure, ZIF-12. The solvent selection can potentially influence the morphology and porosity of the ZIFs. The solvent must affect factors like particle size, pore size distribution, and the overall crystallinity of the ZIFs. These morphological variations could, in turn, influence the electrochemical performance of supercapacitors.

Interestingly, the sample synthesised with bIM in GVL demonstrated the highest capacitance value among the tested electrodes. This finding suggests that combining the bIM linker and GVL solvent might be favourable for achieving enhanced supercapacitive performance. It is particularly noteworthy that the sample exhibits a ZIF-12-like structure, which belongs to the RHO phase. Compared to the more common ZIF-67 (Co-mIM) and ZIF-9 (Co-bIM) structures, ZIF-12 offers potential advantages for supercapacitors due to its larger pore size and potentially higher surface area. These factors can facilitate better electrolyte ion accessibility and enhance the overall capacitance. This study's use of bio-derived solvents (Cyrene^{TM} and GVL) holds promise for developing more sustainable MOF-based supercapacitors. Future research could explore the potential of these bio-solvents for synthesising other high-performance cobalt ZIFs for supercapacitor applications. GCD measurements revealed a strong influence of solvent on ZIF-67 capacitance. ZIF-67(GVL) displayed the highest specific capacitance (C_{sp}) of 39 F g^{-1} at 1 A g^{-1}, 2.4 times greater than ZIF-67(DMF) and over six times higher than ZIF-67(Cyrene). ZIF-9 electrodes exhibited a lower C_{sp} compared to ZIF-67 across all solvents. Remarkably, ZIF-12(GVL) achieved an exceptional C_{sp} of 44 F g^{-1} at 1 A g^{-1}, surpassing all other ZIFs. These results highlight the crucial role of solvent and framework topology in optimising ZIF electrode performance for supercapacitors.

5. Conclusions

The present study demonstrates the influence of linker selection (mIM and bIM) and solvent choice (DMF, Cyrene^{TM}, GVL) on the structure and supercapacitor performance of cobalt ZIFs. Notably, the ZIF-12 structure obtained with bIM in GVL delivered the highest capacitance among the tested electrodes. This suggests the potential of this specific combination for achieving enhanced supercapacitive performance, likely due to the larger pore size and potentially higher surface area offered by the RHO structure. ZIF-12 emerged as the supercapacitor electrode, achieving a remarkable specific capacitance (C_{sp}) of 44 F g^{-1} at 1 A g^{-1}. Even at higher current densities, ZIF-12(GVL) maintained superior C_{sp}, demonstrating a high-rate capability of the ZIF-12 electrode, respectively. The combined effect of solvent choice (GVL) and the unique RHO-type topology of ZIF-12 likely contribute to this exceptional energy storage performance. Further investigations are necessary to elucidate the structure–performance relationship at a deeper level. The successful utilisation of bio-derived solvents also opens exciting avenues for developing sustainable MOF-based supercapacitors. Exploring the potential of these green alternatives for synthesising high-performance cobalt ZIFs is a promising direction for future research.

Author Contributions: Conceptualisation, S.D.W.; methodology, S.D.W.; formal analysis, V.M.; investigation, V.M.; data curation, V.M.; writing—original draft preparation, V.M.; writing—review and editing, V.M., B.C., V.N.-V., and S.D.W.; supervision, V.N.-V. and S.D.W. All authors have read and agreed to the published version of the manuscript.

Funding: V.M. acknowledges Aston University EPS College—Ph.D. studentship.

Institutional Review Board Statement: Not applicable.

Informed Consent Statement: Not applicable.

Data Availability Statement: Raw X-ray diffraction and scanning electron microscopy data are available on request.

Conflicts of Interest: The authors declare no conflicts of interest.

Appendix A

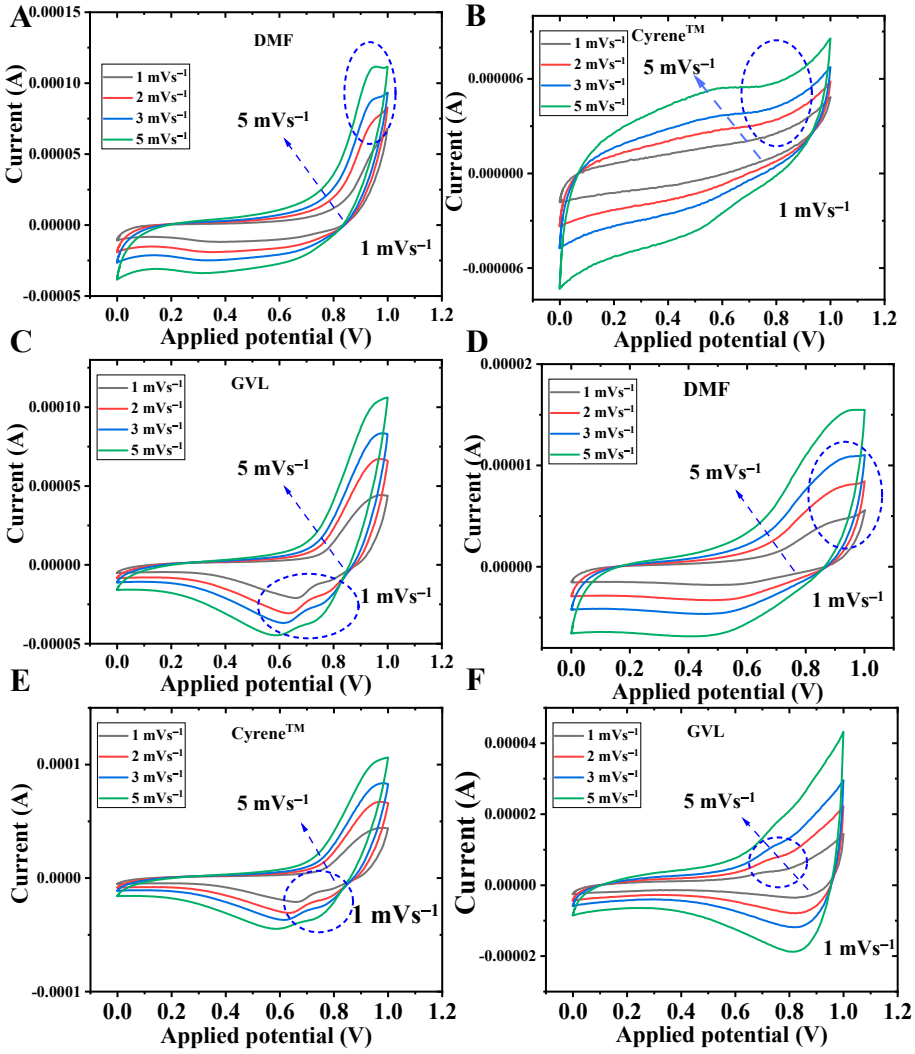

Figure A1. Cyclic voltammetry current vs. applied potential profile at lower scan rates (1 mVs^{-1} to 5 mV s^{-1}) for Co-mIM ZIFs in (**A**) DMF, (**B**) CyreneTM, (**C**) GVL, and Co-bIM ZIFs in (**D**) DMF, (**E**), Cyrene™, and (**F**) GVL.

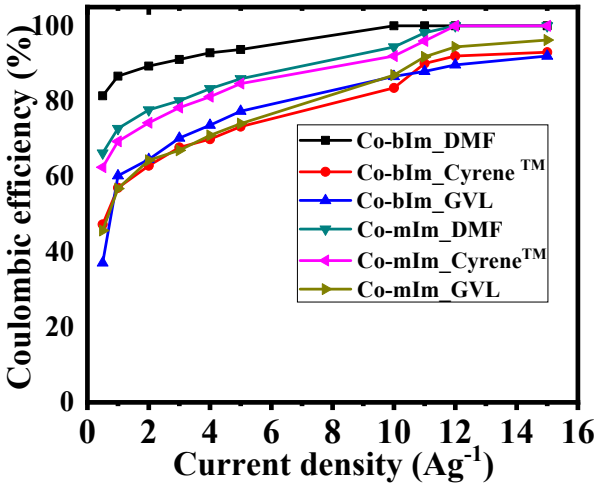

Figure A2. Coloumbic efficiency vs. current density of the supercapacitor electrodes.

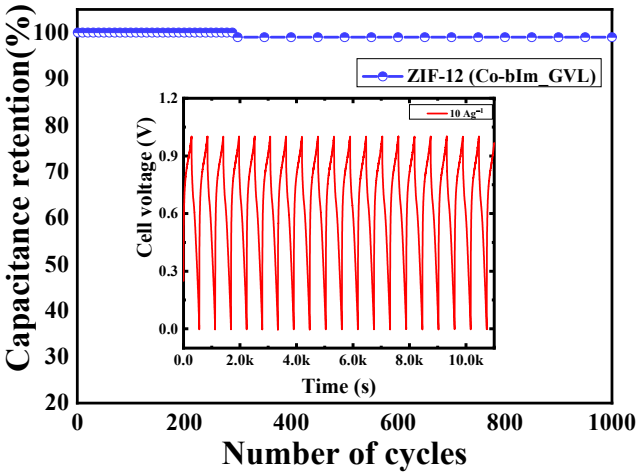

Figure A3. Cycle stability of ZIF-12 electrodes at current density of 10 Ag^{-1}.(Insert: GCD profile of first few cycles).

References

1. Citarella, A.; Amenta, A.; Passarella, D.; Micale, N. Cyrene: A Green Solvent for the Synthesis of Bioactive Molecules and Functional Biomaterials. *Int. J. Mol. Sci.* **2022**, *23*, 15960. [CrossRef] [PubMed]
2. Stini, N.A.; Gkizis, P.L.; Kokotos, C.G. Cyrene: A bio-based novel and sustainable solvent for organic synthesis. *Green Chem.* **2022**, *24*, 6435–6449. [CrossRef]
3. Clark, J.H.; Farmer, T.J.; Hunt, A.J.; Sherwood, J. Opportunities for Bio-Based Solvents Created as Petrochemical and Fuel Products Transition towards Renewable Resources. *Int. J. Mol. Sci.* **2015**, *16*, 17101–17159. [CrossRef]
4. Clarke, C.J.; Tu, W.C.; Levers, O.; Brohl, A.; Hallett, J.P. Green and Sustainable Solvents in Chemical Processes. *Chem. Rev.* **2018**, *118*, 747–800. [CrossRef] [PubMed]
5. Winterton, N. The green solvent: A critical perspective. *Clean. Technol. Environ. Policy* **2021**, *23*, 2499–2522. [CrossRef]
6. Calvo-Flores, F.G.; Monteagudo-Arrebola, M.J.; Dobado, J.A.; Isac-Garcia, J. Green and Bio-Based Solvents. *Top. Curr. Chem.* **2018**, *376*, 18. [CrossRef] [PubMed]
7. Farran, A.; Cai, C.; Sandoval, M.; Xu, Y.; Liu, J.; Hernaiz, M.J.; Linhardt, R.J. Green solvents in carbohydrate chemistry: From raw materials to fine chemicals. *Chem. Rev.* **2015**, *115*, 6811–6853. [CrossRef]
8. Clark, J.H.; El Deswarte, F.I.; Farmer, T.J. The integration of green chemistry into future biorefineries. *Biofuels Bioprod. Biorefining* **2008**, *3*, 72–90. [CrossRef]
9. Gao, F.; Bai, R.; Ferlin, F.; Vaccaro, L.; Li, M.; Gu, Y. Replacement strategies for non-green dipolar aprotic solvents. *Green Chem.* **2020**, *22*, 6240–6257. [CrossRef]
10. Jordan, A.; Hall, C.G.J.; Thorp, L.R.; Sneddon, H.F. Replacement of Less-Preferred Dipolar Aprotic and Ethereal Solvents in Synthetic Organic Chemistry with More Sustainable Alternatives. *Chem. Rev.* **2022**, *122*, 6749–6794. [CrossRef]
11. Camp, J.E. Bio-available Solvent Cyrene: Synthesis, Derivatization, and Applications. *ChemSusChem* **2018**, *11*, 3048–3055. [CrossRef]
12. Wang, Y.; Dai, M.; Luo, G.; Fan, J.; Clark, J.H.; Zhang, S. Preparation and Application of Green Sustainable Solvent Cyrene. *Chemistry* **2023**, *5*, 2322–2346. [CrossRef]
13. Vijayakumar, M.; Adduru, J.; Rao, T.N.; Karthik, M. Conversion of Solar Energy into Electrical Energy Storage: Supercapacitor as an Ultrafast Energy-Storage Device Made from Biodegradable Agar-Agar as a Novel and Low-Cost Carbon Precursor. *Glob. Chall.* **2018**, *2*, 1800037. [CrossRef]
14. Vijayakumar, M.; Bharathi Sankar, A.; Sri Rohita, D.; Nanaji, K.; Narasinga Rao, T.; Karthik, M. Achieving High Voltage and Excellent Rate Capability Supercapacitor Electrodes Derived From Bio-renewable and Sustainable Resource. *ChemistrySelect* **2020**, *5*, 8759–8772. [CrossRef]
15. Tahir, M.A.; Arshad, N.; Akram, M. Recent advances in metal organic framework (MOF) as electrode material for super capacitor: A mini review. *J. Energy Storage* **2022**, *47*, 103530. [CrossRef]
16. Zhang, A.; Zhang, Q.; Fu, H.; Zong, H.; Guo, H. Metal-Organic Frameworks and Their Derivatives-Based Nanostructure with Different Dimensionalities for Supercapacitors. *Small* **2023**, *19*, e2303911. [CrossRef] [PubMed]
17. Saleem, M.; Ahmad, F.; Fatima, M.; Shahzad, A.; Javed, M.S.; Atiq, S.; Khan, M.A.; Danish, M.; Munir, O.; Arif, S.M.B.; et al. Exploring new frontiers in supercapacitor electrodes through MOF advancements. *J. Energy Storage* **2024**, *76*, 109822. [CrossRef]
18. Wang, K.-B.; Xun, Q.; Zhang, Q. Recent progress in metal-organic frameworks as active materials for supercapacitors. *EnergyChem* **2020**, *2*, 100025. [CrossRef]
19. He, H.; Li, R.; Yang, Z.; Chai, L.; Jin, L.; Alhassan, S.I.; Ren, L.; Wang, H.; Huang, L. Preparation of MOFs and MOFs derived materials and their catalytic application in air pollution: A review. *Catal. Today* **2021**, *375*, 10–29. [CrossRef]

20. Xie, Y.; Wu, X.; Shi, Y.; Peng, Y.; Zhou, H.; Wu, X.; Ma, J.; Jin, J.; Pi, Y.; Pang, H. Recent Progress in 2D Metal-Organic Framework-Related Materials. *Small* **2024**, *20*, e2305548. [CrossRef]
21. Wang, K.; Li, Y.; Xie, L.-H.; Li, X.; Li, J.-R. Construction and application of base-stable MOFs: A critical review. *Chem. Soc. Rev.* **2022**, *51*, 6417–6441. [CrossRef] [PubMed]
22. Seth, S.; Matzger, A.J. Metal–Organic Frameworks: Examples, Counterexamples, and an Actionable Definition. *Cryst. Growth Des.* **2017**, *17*, 4043–4048. [CrossRef]
23. Soni, S.; Bajpai, P.K.; Arora, C. A review on metal-organic framework: Synthesis, properties and application. *Charact. Appl. Nanomater.* **2020**, *3*, 87–106. [CrossRef]
24. Zhou, H.C.; Long, J.R.; Yaghi, O.M. Introduction to metal-organic frameworks. *Chem. Rev.* **2012**, *112*, 673–674. [CrossRef] [PubMed]
25. Radhakrishnan, S.; Selvaraj, S.C.; Kim, B.-S. Morphology engineering of Co-MOF nanostructures to tune their electrochemical performances for electrocatalyst and energy-storage applications supported by DFT studies. *Appl. Surf. Sci.* **2022**, *605*, 154691. [CrossRef]
26. Yap, M.H.; Fow, K.L.; Chen, G.Z. Synthesis and applications of MOF-derived porous nanostructures. *Green Energy Environ.* **2017**, *2*, 218–245. [CrossRef]
27. Bhindi, M.; Massengo, L.; Hammerton, J.; Derry, M.J.; Worrall, S.D. Structure Control Using Bioderived Solvents in Electrochemical Metal-Organic Framework Synthesis. *Appl. Sci.* **2023**, *13*, 720. [CrossRef]
28. Flügel, E.A.; Ranft, A.; Haase, F.; Lotsch, B.V. Synthetic routes toward MOF nanomorphologies. *J. Mater. Chem.* **2012**, *22*, 10119–10133. [CrossRef]
29. Li, W.-J.; Tu, M.; Cao, R.; Fischer, R.A. Metal–organic framework thin films: Electrochemical fabrication techniques and corresponding applications & perspectives. *J. Mater. Chem. A* **2016**, *4*, 12356–12369. [CrossRef]
30. Xiao, X.; Zou, L.; Pang, H.; Xu, Q. Synthesis of micro/nanoscaled metal-organic frameworks and their direct electrochemical applications. *Chem. Soc. Rev.* **2020**, *49*, 301–331. [CrossRef]
31. Al Obeidli, A.; Ben Salah, H.; Al Murisi, M.; Sabouni, R. Recent advancements in MOFs synthesis and their green applications. *Int. J. Hydrogen Energy* **2022**, *47*, 2561–2593. [CrossRef]
32. He, Q.; Zhan, F.; Wang, H.; Xu, W.; Wang, H.; Chen, L. Recent progress of industrial preparation of metal–organic frameworks: Synthesis strategies and outlook. *Mater. Today Sustain.* **2022**, *17*, 100104. [CrossRef]
33. Li, Z.; Smith, K.H.; Stevens, G.W. The use of environmentally sustainable bio-derived solvents in solvent extraction applications—A review. *Chin. J. Chem. Eng.* **2016**, *24*, 215–220. [CrossRef]
34. Guo, X.; Xing, T.; Lou, Y.; Chen, J. Controlling ZIF-67 crystals formation through various cobalt sources in aqueous solution. *J. Solid State Chem.* **2016**, *235*, 107–112. [CrossRef]
35. Qian, J.; Sun, F.; Qin, L. Hydrothermal synthesis of zeolitic imidazolate framework-67 (ZIF-67) nanocrystals. *Mater. Lett.* **2012**, *82*, 220–223. [CrossRef]
36. He, M.; Yao, J.; Liu, Q.; Zhong, Z.; Wang, H. Toluene-assisted synthesis of RHO-type zeolitic imidazolate frameworks: Synthesis and formation mechanism of ZIF-11 and ZIF-12. *Dalton Trans.* **2013**, *42*, 16608–16613. [CrossRef] [PubMed]
37. Duong, A.T.A.; Nguyen, H.V.; Tran, M.V.; Ngo, Q.N.; Luu, L.C.; Doan, T.L.H.; Nguyen, H.N.; Nguyen, M.V. Influence of ZIF-9 and ZIF-12 structure on the formation of a series of new Co/N-doped porous carbon composites as anode electrodes for high-performance lithium-ion batteries. *RSC Adv.* **2023**, *13*, 17370–17383. [CrossRef]
38. Cao, W.; Han, M.; Qin, L.; Jiang, Q.; Xu, J.; Lu, Z.; Wang, Y. Synthesis of zeolitic imidazolate framework-67 nanocube wrapped by graphene oxide and its application for supercapacitors. *J. Solid State Electrochem.* **2018**, *23*, 325–334. [CrossRef]
39. Zhang, W.; Tan, Y.; Gao, Y.; Wu, J.; Hu, J.; Stein, A.; Tang, B. Nanocomposites of zeolitic imidazolate frameworks on graphene oxide for pseudocapacitor applications. *J. Appl. Electrochem.* **2016**, *46*, 441–450. [CrossRef]
40. Hou, X.; Zhang, Y.; Dong, Q.; Hong, Y.; Liu, Y.; Wang, W.; Shao, J.; Si, W.; Dong, X. Metal Organic Framework Derived Core–Shell Structured Co9S8@N–C@MoS2 Nanocubes for Supercapacitor. *ACS Appl. Energy Mater.* **2018**, *1*, 3513–3520. [CrossRef]
41. Duan, C.; Yu, Y.; Hu, H. Recent progress on synthesis of ZIF-67-based materials and their application to heterogeneous catalysis. *Green Energy Environ.* **2022**, *7*, 3–15. [CrossRef]
42. Dai, J.; Xiao, S.; Liu, J.; He, J.; Lei, J.; Wang, L. Fabrication of ZIF-9@super-macroporous microsphere for adsorptive removal of Congo red from water. *RSC Adv.* **2017**, *7*, 6288–6296. [CrossRef]
43. Zhang, L.; Guo, Y.; Shen, K.; Huo, J.; Liu, Y.; Guo, S. Ion-matching porous carbons with ultra-high surface area and superior energy storage performance for supercapacitors. *J. Mater. Chem. A* **2019**, *7*, 9163–9172. [CrossRef]
44. Lobato, B.; Suárez, L.; Guardia, L.; Centeno, T.A. Capacitance and surface of carbons in supercapacitors. *Carbon* **2017**, *122*, 434–445. [CrossRef]
45. Park, K.S.; Ni, Z.; Côté, A.P.; Choi, J.Y.; Huang, R.; Uribe-Romo, F.J.; Chae, H.K.; O'Keeffe, M.; Yaghi, O.M. Exceptional chemical and thermal stability of zeolitic imidazolate frameworks. *Proc. Natl. Acad. Sci. USA* **2006**, *103*, 10186–10191. [CrossRef]